Department of Energy Small Business Innovation Research

Phase I Final Technical Report

Title: Development and Characterization of a Thermodenuder for Aerosol Volatility Measurements

Report #: DOE/ER/85161

DOE Award/Contract Number: DE-FG02-08ER85161

Aerodyne Report #: RP-10531.1

Recipient/contractor (organization): Aerodyne Research, Inc., 45 Manning Rd., Billerica, MA 01821-3976

Principal Investigator: Dr. Timothy Onasch

Email address: onasch@aerodyne.com

Report Date: September 9, 2009

Reporting Period: 6/30/08 - 3/29/09

Sponsoring DOE Program Office: DOE SBIR

Recipient/Contractor Point of Contact: Dr. Timothy Onasch

Abstract:

This SBIR Phase I project addressed the critical need for improved characterization of carbonaceous aerosol species in the atmosphere. The proposed work focused on the development of a thermodenuder (TD) system capable of systematically measuring volatility profiles of primary and secondary organic aerosol species and providing insight into the effects of absorbing and nonabsorbing organic coatings on particle absorption properties. This work provided the fundamental framework for the generation of essential information needed for improved predictions of ambient aerosol loadings and radiative properties by atmospheric chemistry models. As part of this work, Aerodyne Research, Inc. (ARI) continued to develop and test, with the final objective of commercialization, an improved thermodenuder system that can be used in series with any aerosol instrument or suite of instruments (e.g., aerosol mass spectrometers-AMS, scanning mobility particle sizers-SMPS, photoacoustic absorption spectrometers-PAS, etc.) to obtain aerosol chemical, physical, and optical properties as a function of particle volatility. In particular, we provided the proof of concept for the direct coupling of our improved TD design with a full microphysical model to obtain volatility profiles for different organic aerosol components and to allow for meaningful comparisons between different TD-derived aerosol measurements.

In a TD, particles are passed through a heated zone and a denuding (activated charcoal) zone to remove semi-volatile material. Changes in particle size, number concentration, optical absorption, and chemical composition are subsequently detected with aerosol instrumentation. The aerosol volatility profiles provided by the TD will strengthen organic aerosol emission inventories, provide further insight into secondary aerosol formation mechanisms, and provide an important measure of particle absorption (including brown carbon contributions and identification, and absorption enhancements due to coatings on soot particles).

The successfully completed Phase I project included construction of a prototype design for the TD with detailed physical modeling, testing with laboratory and ambient aerosol particles, and the initiation of a detailed microphysical model of the aerosol particles passing through the TD to extract vapor pressure distributions. The objective of the microphysical model is to derive vapor pressure distributions (i.e. vapor pressure ranges, including single chemical compounds, mixtures of known compounds, and complex ‘real-world’ aerosols, such as SOA, and soot particles with absorbing and nonabsorbing coatings) from TD measurements of changes in particle size, mass, and chemical composition for known TD temperatures and flow rates (i.e. residence times). The proposed Phase II project was designed to optimize several TD systems for different instrument applications and to combine the hardware and modeling into a robust package for commercial sales.

Report:

Significance and Background Information

Recent field campaigns [*Lelieveld, et al.*, 2001; *Stone, et al.*, 2007], coupled with modeling studies [*Menon, et al.*, 2002; *Ramanathan, et al.*, 2001; *Ramanathan, et al.*, 2007a], have highlighted the substantial effects that anthropogenic carbonaceous aerosols may have on the earth's climate. Organic compounds make up a large fraction of atmospheric fine particulate matter, accounting for 20-90% of aerosol mass in the lower troposphere [*Kanakidou, et al.*, 2005]. Because of their implications for human health, urban pollution, and global climate, it is important that atmospheric loadings of carbonaceous aerosol particles be accurately modeled. This requires a detailed, quantitative characterization of their sources, effects, and fates in the atmosphere. This includes their radiative properties, as the "uncertainty in total anthropogenic radiative forcing (greenhouse gases + aerosols) is dominated by the uncertainty in aerosol radiative forcing" [*Chin, et al.*, 2009]. Given the large number and variability of chemical constituents (e.g., [*Hamilton, et al.*, 2004]), potential sources, and atmospheric chemical transformations of carbonaceous aerosol, such characterization presents a substantial experimental and theoretical challenge.

Carbonaceous aerosols in the atmosphere include primary organic (e.g., lubricating oils from internal combustion engines), primary soot (e.g., elemental carbon + organic material from combustion, biomass/biofuel burning), and secondary organic aerosol generated from the photochemistry of precursor volatile organic compounds (VOC; e.g., biogenic emissions, volatilized hydrocarbon fuels, and industrial emissions) [*Fuzzi, et al.*, 2006; *Jacobson, et al.*, 2000]. Several recent studies have shown that our ability to accurately model secondary organic aerosol (SOA) formation and evolution is severely limited. State-of-the-art atmospheric chemistry models predict SOA loadings which are generally far lower (by an order of magnitude or more) than is measured. Such discrepancies appear to be ubiquitous, as they are found for a variety of models over a wide range of atmospheric conditions, including urban [*Volkamer, et al.*, 2006], marine [*de Gouw, et al.*, 2005], rural [*Johnson, et al.*, 2006], and remote [*Heald, et al.*, 2005] regions. In all cases, the discrepancy between measured and modeled aerosol loadings appears to be a result of a large underprediction of SOA formation, in agreement with aerosol mass spectrometer (AMS) measurements which consistently find highly oxidized organics to dominate the organic fraction of the aerosol [*Zhang, et al.*, 2007].

These results suggest that widely-used theoretical treatments are insufficient to accurately represent the behavior of tropospheric particles. The standard framework for describing atmospheric organic aerosol is that primary organic aerosol (POA) is completely nonvolatile, remaining in the atmosphere until removed by physical processes (wet or dry deposition), whereas secondary organic aerosol (SOA), formed by the oxidation of a small handful of hydrocarbons, is semivolatile, with components present in both the gas and particle phases. However, recent work has shown that this picture may be fundamentally incorrect, as primary organic aerosol particles (such as wood smoke and diesel exhaust) decrease in mass upon dilution, and so are actually composed of semivolatile organics [*Shrivastava, et al.*, 2006]. SOA, by contrast, is well-established to be governed by the formation and partitioning of semivolatile organics. However recent

work by Robinson et al. [2007] shows that in addition to traditional SOA precursors (VOCs such as aromatics and terpenes), lower volatility gas-phase organics may also oxidize to efficiently form SOA.

As a result, it is now clear that the volatility of organic aerosol species determines the chemical composition and mass loading of all atmospheric organic aerosol (both SOA and POA) [*Donahue, et al.*, 2006; *Robinson, et al.*, 2007]. In order to successfully model organic aerosol emissions and atmospheric loadings, the partitioning of organic compounds between the particle and gas phases (determined by their vapor pressures) must be-well characterized. However, the vapor pressures of most low-volatility organic species found in the atmosphere are very poorly constrained. Recent work has focused on the volatility of individual compounds [*Bilde and Pandis*, 2001; *Cappa, et al.*, 2007; *Chattopadhyay, et al.*, 2001; *Chattopadhyay and Ziemann*, 2005], though the lack of chemical speciation of the vast majority of atmospherically relevant particulate organics severely limits such an approach. Donahue et al. [2006] introduced an approach to model the "volatility distribution" of complex mixtures of organic aerosol, such as emissions from a combustion system or the products in SOA, by binning components by vapor pressures and modeling the physical and chemical evolution of the binned organics. Thus, instrumentation that can directly measure organic aerosol volatility distributions will generate output that can be directly used in local, regional, and global models. We plan to deploy a TD-AMS during the DOE ASP Carbonaceous Aerosols and Radiative Effects Study (CARES) 2010 project in Sacramento valley as a demonstration of this TD technology in support of the DOE ASP program.

While volatility distributions provide the information necessary to model aerosol mass concentrations, the systematic study of the effect of volatile particle coatings on aerosol radiative properties can provide necessary information for prediction of aerosol radiative properties. The black carbon (BC) fraction of carbonaceous aerosol has particularly important implications for climate, as it is a strong absorber of incoming solar radiation. Recent global inventories of combustion sources put black carbon emissions at around 8 Tg/yr and organic carbon (OC) emissions at around 34 Tg/yr [*Bond, et al.*, 2004], and it has been estimated that the direct radiative effect of BC is the second-most important contributor to global warming after absorption by CO_2 [*Jacobson*, 2004; *Ramanathan and Carmichael*, 2008; *Solomon, et al.*, 2007]. However, estimating the contribution of black carbon to global climate change has become more complicated with the realization that coatings can enhance the absorption cross section of the black carbon particles [*Bond, et al.*, 2006; *Schnaiter, et al.*, 2005; *Schwarz, et al.*, 2008] and other light-absorbing carbonaceous particles are present in the atmosphere, e.g., brown carbon [*Andreae and Gelencser*, 2006]. Black carbon particles are often found in mixtures of light-absorbing and light-scattering aerosols, i.e., atmospheric brown clouds [*Ramanathan, et al.*, 2007b]. Atmospheric brown clouds contribute to both atmospheric solar heating and surface cooling. In order to sort out the chemical composition and resulting absorption cross sections for ambient carbonaceous aerosol, new techniques are required.

Aerodyne Research, Inc. (ARI) has recently built a thermodenuder (EPA Star R831080) in collaboration with researchers at UC Riverside and the University of Colorado based on the design by Wehner et al. [2002b] and improved on the design,

specifically with respect to temperature and flow control, as part of this DOE Phase I project. The thermodenuder was designed originally to operate in front of an Aerosol Mass Spectrometer (AMS), allowing for real-time chemically- and size-resolved mass loading measurements as a function of particle volatility. Phase I laboratory and modeling results have shown that the current design can be operated under different flow rates (i.e., using more aerosol instruments than just an AMS) and for a range of aerosol particles sizes and number concentrations and still provide the same volatility information, thus making the thermodenuder more widely applicable. Modified forms of the Wehner et al. [2002b] thermodenuder design have been successfully operated in series with aerosol mass spectrometers by several research groups on ambient aerosol in California (SOAR 2006) [*Denkenberger, et al.*, 2007], Mexico City (2006) [*Huffman, et al.*, 2009a], during biomass burning experiments at the National Fire Science Laboratory in Missoula Montana (FLAME I and II, 2006, 2007), and on laboratory generated particles [*Wu, et al.*, 2009]. The combination of the chemical and volatility measurements of the combined instrumentation (TD-AMS) has already yielded substantial insight into differences in volatility of various ambient and laboratory aerosols; for example it has shown that POA is generally more volatile than SOA, in contrast to the treatments by most atmospheric models [*Huffman, et al.*, 2007].

Information about the influence of volatile organic coatings on aerosol radiative properties can be similarly obtained by combining the TD with instruments that measure aerosol absorption and/or extinction. As an example, in related work, we have proposed to operate an AMS and a photoacoustic instrument simultaneously behind a thermodenuder during the NOAA CalNex 2010 study. The combination of these two real-time instruments measuring the chemical composition and absorption of the carbonaceous aerosol (including ambient and ship plume exhaust) will provide important insights into absorption enhancement factors and the potential quantification and identification of brown carbon material and sources.

Thermodenuders

Thermodenuder (TD) methods involve exposing aerosol to an elevated temperature, promoting the evaporation of the more volatile components and analyzing the remaining aerosol (consisting of lower-volatility components). TD designs can be as simple as a heated tube [*Clarke, et al.*, 1987] or may contain multiple heating regions followed by a desorption region. The latter style thermodenuders are designed to allow for wider ranges in sampled mass loadings and faster sample flow rates and, thus, are applicable to a wider range of aerosol instrumentation.

Burtscher et al. [2001] developed a thermodesorber for atmospheric aerosol and combustion exhaust emission studies with a residence time of

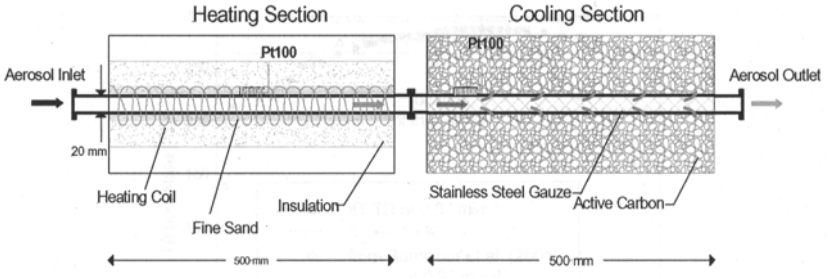

Figure 1. Thermodenuder design of Wehner et al. [2002a].

~3 seconds. This initial work detailed the two element design (heating and denuding zones) and set the standard for testing TD systems as a function of axial temperature profiles, particle losses due to sedimentation, diffusion, and thermophoresis, and aerosol and cooling flow rates. Wehner et al. [2002a] developed an improved thermodenuder, based on the Burtscher et al. [2001] design, but with several improvements to the heating and cooling profiles and longer residence times from 6-9 seconds. This design is shown in Figure 1. Subsequent work by An et al.[2007] explored the use of a heating zone with substantially longer residence times (up to 15.8 seconds) for laboratory measurements. Results from this work were highly dependent on residence time, with lower residence times (such as is typical for a volatility tandem differential mobility analyzer, or VTDMA) leading to much less vaporization. Consequently, inferred nonvolatile fractions are overestimated [*Baltensperger, et al.*, 2005; *Kalberer, et al.*, 2004]. A novel approach by Fierz et al [2007] has also investigated the use of three regions (heated, heated desorption, and desorption), as opposed to the two regions in the Wehner et al. [2002a] design. The goal of this design was to limit recondensation of hot gases on sample particles during the transition between the heated and desorption regions.

There are two commercially available thermodenuders, from TSI Inc. (model 3065; originally the TOPAS design; low-flow thermodenuder with optimal flow range from 0.5 to 1.0 lpm and a maximum temperature of 400°C) and Dekati Ltd. (models ELA-111 and ELA-230; designed to remove volatile and semi-volatile compounds from combustion exhaust at flow rates of 10-20 lpm with maximum temperature of 300°C). These systems were built for specific purposes (e.g., to interface with Dekati ELPI and DMM-230 instruments) and thus are limited in their flexibility to be used with different systems/instrumentation [*Madl*, 2003]. Furthermore, as discussed by An et al. [2007], the commercial models have short residence times (0.3 s for the Dekati and 1-1.5 s for the TSI TD) that do not allow enough time for low-volatility compounds to evaporate from sampled aerosol particles, precluding quantitative measurement of vapor pressures. There is thus currently a specific need in the aerosol community for a commercially-available, research-grade thermodenuder which may be used with a range of aerosol instrumentation. As a case in point, the most recent work on aerosol volatility measurements has been done using custom-built thermodenuders that are not commercially available [*An, et al.*, 2007; *Denkenberger, et al.*, 2007; *Huffman, et al.*, 2007; *Wehner, et al.*, 2004].

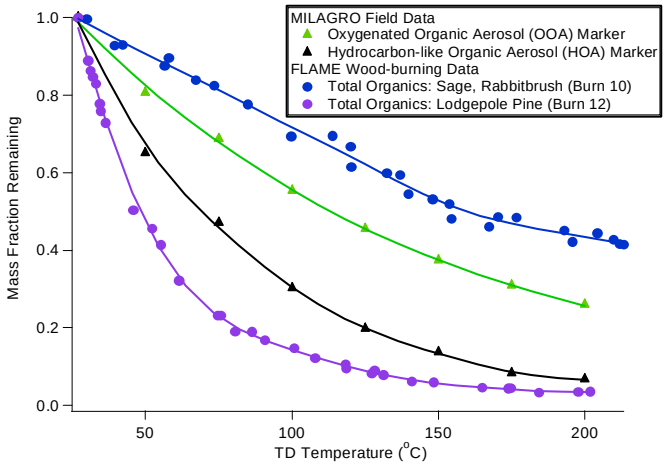

Figure 2. Example of the ability of the TD-AMS system to measure the volatility spectrum of a range of organic species, taken from field measurements in Mexico City and controlled burn lab tests during the FLAME project.

In 2005, Aerodyne Research, Inc., in collaboration with UC Riverside and U Colorado,

Boulder, built a prototype thermodenuder system to be used in conjunction with online measurements of aerosol composition (the Aerodyne Aerosol Mass Spectrometer [*Jayne, et al.*, 2000] and Temperature Desorption Particle Beam Mass Spectrometer [*Tobias and Ziemann*, 1999]), in order to yield particle chemical information as a function of particle volatility. The TD system was built to work as either a field or laboratory instrument. The TD, based on the design by Wehner et al. [2002a], consists of a 1 inch stainless steel tube wrapped with heating tape and insulated with fiberglass encased in a stainless steel shell. The TD has three heating zones and used multiple thermocouples along the tube wall path to monitor the uniformity of the temperature field. The oven temperature is controlled with PID temperature controllers. The system was optimized for low flow (~0.5 to 1.0 lpm) conditions, a residence time of ~10 seconds in the heating zone, and relatively low temperatures (<300^{o}C) to minimize potential charring of organic aerosols. A detailed description of this thermodenuder has been published [*Huffman, et al.*, 2008; *Huffman, et al.*, 2009b].

Thermodenuder techniques have been employed in the characterization of various aerosol types, including emissions from combustion [*Biswas, et al.*, 2007; *Wehner, et al.*, 2004], laboratory-generated SOA and Humic acids [*An, et al.*, 2007; *Meyer, et al.*, 2009; *Wu, et al.*, 2009], and ambient aerosol [*Denkenberger, et al.*, 2007; *Huffman, et al.*, 2009a; *Wehner, et al.*, 2004]. For example, figure 2 shows a summary of the data from TD-AMS obtained during MILAGRO 2006 and FLAME 2006. The mass fraction remaining after thermodenuding is plotted as a function of TD temperature for a range of different particle types (oxygenated organic aerosol, corresponding to SOA; hydrocarbon-like organic aerosol, corresponding to POA; and organics from the combustion of two biomass samples). A surprising result is that SOA is actually the least volatile organic component in urban air, whereas urban primary organics are found to be substantially more volatile. This is contrary to the parameterization used in current models, in which SOA is treated as semivolatile whereas POA is considered completely non-volatile. Such differences have major implications for the prediction of the fate of carbonaceous aerosol in the atmosphere.

Results such as those shown in Figure 2 have yielded substantial insight into the volatility and chemical composition of carbonaceous aerosols; however, these results have been largely qualitative in nature, describing aerosol components as “more volatile” or “less volatile”. In addition, because of differences between various thermodenuder applications it is not straightforward to compare results from one measurement system to another. To our knowledge the only direct comparison between different volatility measurements of a single system was made by An et al. [2007], in which the volatility of SOA from α-pinene/ NO_x photooxidation was measured with a thermodenuder in series with both an SMPS and a VTDMA system. It was shown that the amount of organic particle mass remaining after heating (corresponding to the lower volatility fraction of the aerosol) varied hugely between the two techniques, which in turn led to dramatically different interpretations of aerosol composition and growth mechanisms.

Thus, the utility of most volatility measurements are currently limited by: (1) the lack of commercially available, research grade thermodenuder designs suitable for use with a wide range of standard aerosol instrumentation, (2) technical issues, such as slow temperature scanning, that make volatility measurements impractical in many cases, (3)

the lack of a theoretical treatment allowing for the quantitative determination of volatility distributions from the raw data, and (4) the resulting inability to quantitatively compare results between different measurements. This phase I project represents an initial investment by DOE into developing a well-characterized, commercially available, research-grade thermodenuder system with potential for widespread, standardized application of this valuable technique.

Degree to which Phase I has Demonstrated Technical Feasibility

We have met or exceeded our goals for the Phase I project. During the Phase I project, a heat and mass transfer model was developed and used to characterize our prototype thermodenuder (TD) system. A modified prototype TD system was built and evaluated in the laboratory for temperature and flow characteristics. Measurements of particle mass loss versus temperature were made with a range of organic and inorganic particles covering a range of vapor pressures. A one dimensional microphysical model was developed using the heat and mass transfer model results. The microphysical model currently includes particle size and number concentration, evaporation and condensation, and particle loss to walls due to diffusion and inertial impaction. The microphysical model was successfully used to derive vapor pressures from laboratory measurements for single component particles.

Phase I, Task 1. Design modeling of the thermodenuder. (100% complete)

The first task of the Phase I project was to develop a simple heat- and mass-transfer model to investigate several important aspects of TD systems. The point of this model is to provide insight into the predicted heat and mass transfer of gas phase molecules inside a TD system to ensure 1) uniform conditions in the heating zone for a range of aerosol flow rates, 2) the ability to rapidly change the temperature in the heating zone from room temperature to ~300^{o}C, and 3) the suppression of potential supersaturation in the denuding zone while the aerosol cools.

The temperature and velocity profiles in the thermodenuder were modeled using FLUENT, a computational fluid dynamics software package, which solves the coupled momentum and energy equations for air. In our simulations, air was modeled as an ideal gas, allowing for density variations with temperature and pressure. The viscosity and thermal conductivity of air were modeled using the kinetic theory of gases. This approach has been shown to be accurate for air in the temperature and pressure ranges of interest -

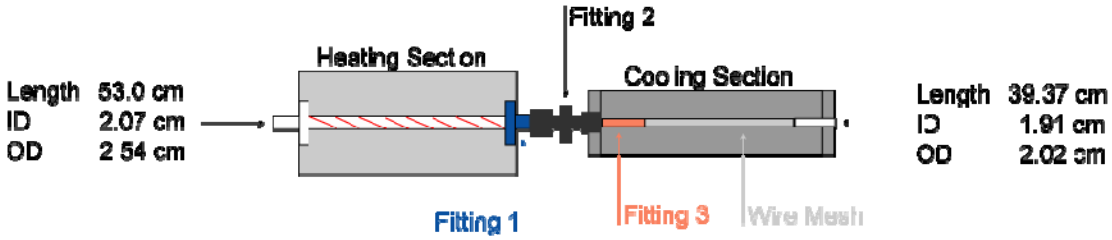

Figure 3: Thermodenuder geometry used in the FLUENT simulations.

namely 25 – 100 °C and ~1 bar [*Chapman, et al.*, 1990]. The heat capacity of air, C_p, was taken to be constant, as observed experimentally for the temperature range of interest. In our simulations, it was assumed that the presence of aerosol particles did not

affect the air flow or temperature profiles. Note that the modeling covered the temperature range up to 100 °C because that is what is relevant for the particular materials studied in the experiments described in Task 3, even though the thermodenuder is physically capable of reaching a temperature of 300 °C.

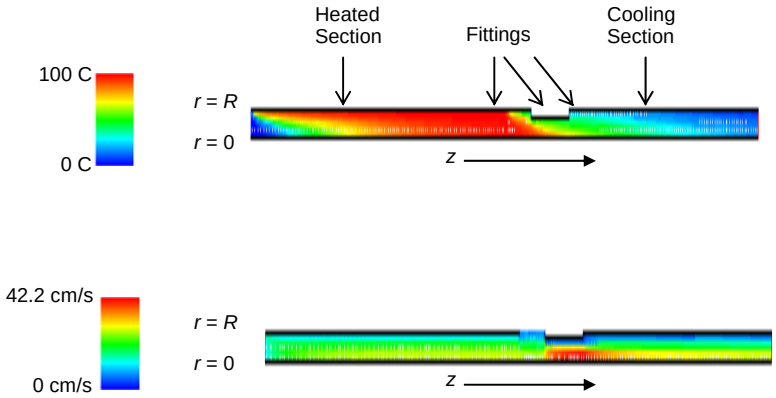

Figure 4: Temperature (top) and axial velocity (bottom) variations in the thermodenuder. The point $r = 0$ corresponds to the centerline and $r = R$ (not drawn to scale) to the walls.

A schematic of the geometry used in our axisymmetric FLUENT model is given in Figure 3 and is based on the prototype TD constructed in this Phase I project. The heating section was modeled as having a constant wall temperature. Air was assumed to enter this section at a temperature of 25 °C with a uniform velocity profile. A natural convection boundary condition was used on the walls of fitting 1 and fitting 2. In the cooling section, the air flow through the activated charcoal was assumed to be negligible compared to the flow within the wire mesh channel. The cooling Section (including fitting 3) was thus modeled as a thick wall containing a static mixture of charcoal and air, with an effective thermal conductivity of 0.12 W/(m·K) corresponding to a charcoal packing density of 430 kg/m^3 [*Prakash, et al.*, 2000]. In all cases, the ambient air temperature was taken to be 25 °C.

Figure 4 shows plots for the temperature and axial velocity profiles for a heating wall temperature of 100 °C and a flow rate of 2.2 SLPM. As expected, there is a transition region for the temperature profile to reach the wall temperature in the heating section, and another transition region for the temperature to drop back to ambient temperature in the cooling section. Due to changes in diameter, there are also transition regions for the velocity profile as the air goes through each fitting/section of the thermodenuder.

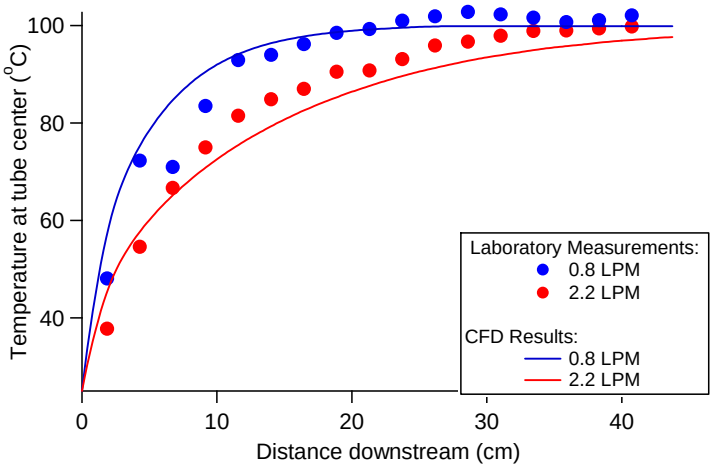

Figure 5. Center line temperature as a function of axial distance calculated by the CFD model (lines) and for experimental measurements (circles).

In order to incorporate the temperature and flow results into our one-dimensional microphysics model, cross-section averages were taken

of the velocity and temperature profiles. In particular, the velocity used in the microphysics model is the cross-section averaged axial velocity, and the temperature used in the microphysics model was the velocity-averaged temperature. A velocity average was used instead of a simple cross-section average temperature in order to account for the different residence times of the aerosol particles traveling along different velocity streamlines. Average velocity and temperature profiles were calculated at three different flowrates – 0.6, 0.8, and 2.2 SLPM, matching the flow rates of the experimental data presented in Task 3. Figure 5 shows the temperature axial profile compared to experimental measurements for two of the flow rates at a wall temperature of 100 °C, and shows good agreement between model and measurements. Agreement could probably be improved with a better scheme for mounting the thermocouple on the center line of the thermodenuder.

Once constructed, the heat- and mass- transfer model was used to understand the optimal operating conditions for the prototype TD. In particular, the residence time inside the heating zone was varied by varying the flow rate in order to understand the range of flow rates over which the center line of the gas flow reaches the wall temperature for the design shown in Figure 3. The model was also used to determine optimal diameter and lengths of the heated and cooled regions for different flow rates associated with different aerosol instrumentation. We discovered that for the flow rates into the AMS (about 0.15 lpm), we could use a much smaller physical size for the TD, making it more attractive to AMS customers. In addition, we discovered that the maximum flow rate through the current design that allows the entire flow to reach the wall temperature (roughly 2 lpm, see Figure 5), is high enough to anticipate running the larger version of the TD in front of a suite of aerosol instrumentation.

Phase I, Task 2. Build prototype TD and develop control software. (100% complete)

During this task, a prototype of the TD was constructed for laboratory evaluation. A bypass line and corresponding automatic valve system were designed and implemented, and improvements were made in the cooling of the heated region.

One of the fundamental measurements using a TD system is the ratio of the particle volume/mass remaining. This ratio is obtained by dividing the aerosol volume/mass after passing through the TD at a given temperature to the aerosol volume/mass under ambient conditions. In some applications, this is done using two detection systems (e.g., two SMPS instruments) [*Wehner, et al.*, 2004]. For practical purposes, this can also be accomplished by automatically switching back and forth

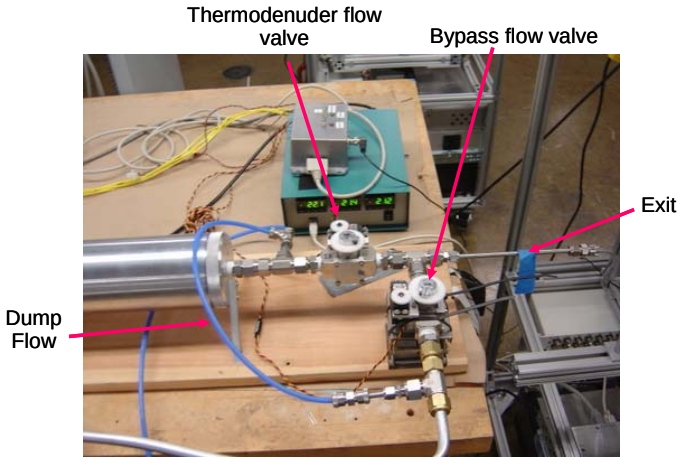

Figure 6. The automated valve switching system for the thermodenuder.

between the TD at a given temperature and a bypass line that is at ambient temperature. By automating this process, the valve switching can be synchronized with the data collection cycle of the aerosol instrumentation. A system of automatic switching valves

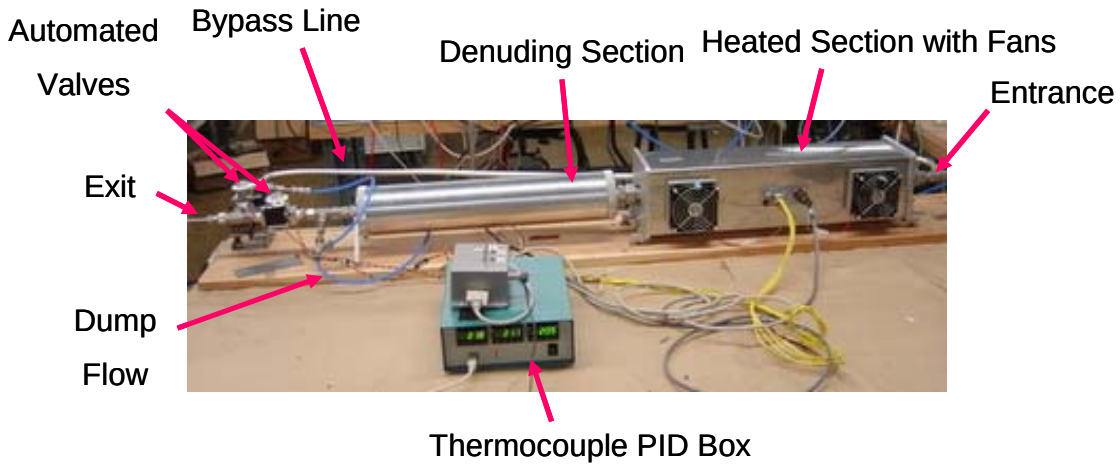

Figure 7. Photograph of the prototype thermodenuder.

was developed for the TD and a photo of the valve system is shown in Figure 6.

The standard operating method for using a thermodenuder has been to sequentially step the temperature inside the heating zone. Another approach has been to utilize several heating zones [*Jonsson, et al.*, 2007] in parallel, operating the heaters at different temperatures, and switching between the heaters during an experiment allowing one to measure 3-4 different temperatures fairly rapidly. During our laboratory and field deployments of the prototype Aerodyne TD system, we have worked out another practical method for operation. This new method relies on a continual ramp of the temperature in the heating zone from low to high temperatures. In order to facilitate timely cooling during the ramp down of temperature in the heating zone, we have implemented a cooling system utilizing fans. We have also made appropriate insulation changes in the heated section of the thermodenuder in order to minimize the effect of the fans on the thermocouples while still enabling the cooling effect of the fans to operate on the outer wall of the heated section. This design has been tested experimentally with temperature profile measurements along the axial center line in the heating zone.

The complete TD system now includes the heating zone, the denuder zone with activated carbon as the adsorbant, a bypass line and an associated automatic valve system. All of these components are controlled using a simple computer interface and controlled through a USB connection. A dump flow was also added which ensures a continuous flow through both the thermodenuder and bypass lines during both valve cycles. Figure 7 shows a photo of the TD system highlighting the various components.

The software developed allows timed temperature profiles to be initiated and controls the switching of the automated sampling and by-pass valves. A ramping rate with minimum and maximum temperatures may be selected or a single temperature value may be set. The user interface for the software is shown in Figure 8a. The software and control electronics also provide data logging capabilities of the temperatures and accessory I/O ports to allow connectivity and communication to and from other

instruments where necessary. These I/O ports are utilized by the AMS in order to synch the menu switching of the AMS with the valve switching of the TD system. Figure 8b shows the correlated temperature ramping cycle and the simultaneous AMS measured ammonium sulfate mass loadings obtained during automatic switching between the by-pass and heated region. The by-pass measurements (blue line) shows uninterrupted mass

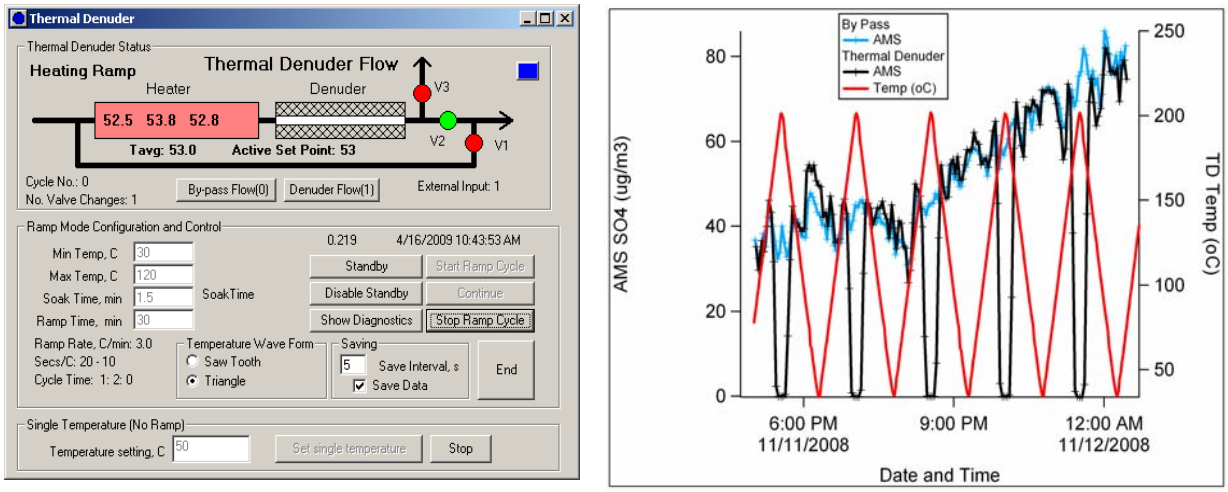

Figure 8. (a) User interface for the software controlling the thermodenuder heating ramp cycle. (b) plot showing a temperature ramp (right axis) and AMS measurements (left axis) in the by-pass and through the heated regions as a function of time.

loadings, whereas the heated aerosol (black line) show complete loss of mass loadings during each elevated temperature section of the ramp cycles. The relevant measurements (ratio of heated to by-pass, examples shown in Figure 10) are directly derived from these correlated measurements.

Phase I, Task 3. Evaluate TD with laboratory and ambient samples. (100% complete)

The focus of Task 3 was to thoroughly test the newly constructed TD system in the laboratory. Following the testing procedures described by Burtscher et al. [2001] and Wehner et al. [2002a], the TD system was tested for axial temperature profiles, particle losses as a function of particle size and heating zone temperature, and for fraction remaining of particle volume/mass for specific individual compounds. The particle

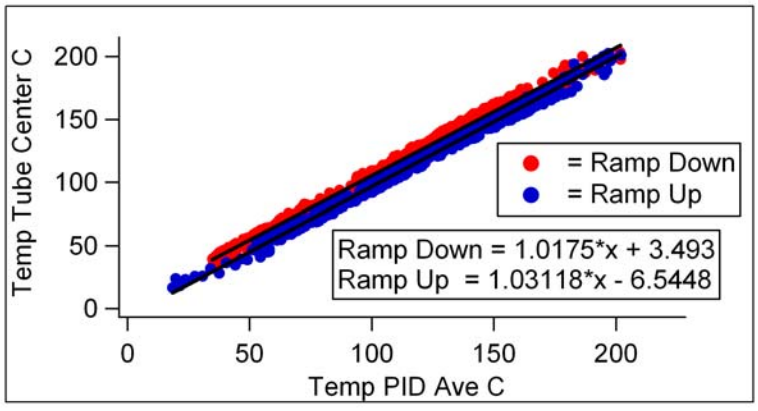

Figure 9. The measured temperature inside the tube at a fixed axial position 23 cm downstream of the entrance to the heated section is plotted versus the average of temperatures measured by three thermocouples placed on the outside wall of the heated section while the temperature is ramped up and down at a rate of 4 °C/min

loss studies for this system have been published by Huffman et al. [*Huffman, et al.*, 2009a; *Huffman, et al.*, 2008].

Temperature measurements were conducted along the length of the heating section of the thermodenuder to determine the relationship between the temperatures read by thermocouples on the outside wall of the heating section with the center tube temperature. Measurements were conducted by moving the thermocouple inside the tube downstream at a given set-point temperature to determine the profile of the temperature inside the tube along the axial center-line (Figure 3). These measurements were used to confirm that the mass- and heat-transfer model developed in Task 1 was doing a reasonable job of representing conditions inside the TD.

Another set of measurements was conducted where the temperature inside the thermodenuder at a fixed point in the heated section was measured during the course of a typical ramping cycle. These measurements were conducted under high and low flow conditions similar to those used during experiments with particles. Initially, all insulation was removed in an attempt to increase the rate of cooling during the ramping cycles. However, this lead to a significant difference between the set point temperature and the measured temperature on the center line, particularly during the cooling phase due to the thermocouples being affected by the air flow from the cooling fans. Based on these measurements, we wrapped just the thermocouples in insulation to protect them from the cooling fan influences, but still allowing for rapid cooling to occur. After these modifications to the insulation, we obtained close agreement between the set point temperatures and the internal temperatures, even for rapid temperature ramps. Typical data is shown in Figure 9. The modified system can now cycle through a temperature ramp from room temperature to 250^{o}C and back in <120 minutes, a factor of ~2 increase in ramp rates.

Figure 10 shows TD data for ammonium sulfate plotted as the ratio of sulfate mass measured with the AMS when the particles pass through the denuder over the sulfate mass when the particles pass through the bypass versus thermodenuder temperature. The thermograms for 100 nm (black points) and 400 nm (green points) particles show that smaller diameter particles evaporate at a lower temperature. The effect of particle diameter is one of the aspects of the thermodenuder operation that was explored with the microphysical model developed in Task 4.

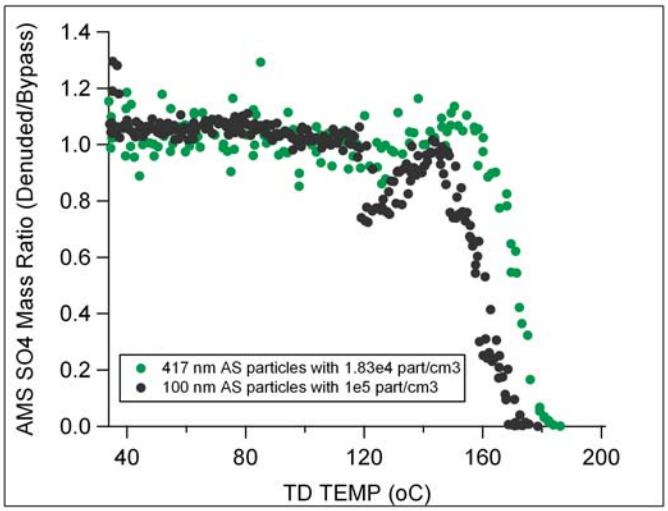

Figure 10. Mass ratio of thermodenuder/bypass mass loadings for ammonium sulfate at 400 and 100 nm.

A series of experiments were conducted where butanedioic (succinic) acid 99% (Aldrich), hexanedioic (adipic) acid 99% (Fluka), decandioic (sebacic) acid 99% (Aldrich) and dioctyl sebacate (DOS) 90% (Aldrich) particles were generated, size selected

with a DMA, run alternatively through the thermodenuder and a bypass line and finally sampled with the AMS, CPC and SMPS systems. DOS was generated by passing filtered air over liquid phase DOS heated in a U-tube at 150° Celsius for high flow measurements and 143° Celsius for low flow measurements. The other organic species were mixed with distilled water and particles were generated with an atomizer and drier. Adipic acid, sebacic acid and DOS experiments were conducted at multiple flow rates in an effort to examine the effect of flow on temperature where particles evaporate in the heated section.

The thermodenuder was operated over the temperature range 30-120 °C with a ramp rate of 3 °C/min for high flow conditions and 1.5° C/min for low flow conditions. The different ramp rates were due to the addition of an SMPS during high flow conditions that required two minute sample rates. The flow was alternated between thermodenuder and bypass flow every 60 seconds during high flow and every 120 seconds during low flow experiments. Thermograms were developed for all experiments by comparing AMS mass loadings ug/m^3 obtained during the thermodenuder flow segments with that obtained during the average of the previous and following bypass segments. That ratio is plotted versus average thermocouple temperature in Figure 11 for sebacic acid. Similar results were obtained for adipic acid and DOS.

Phase I, Task 4. Microphysical model development. (100% complete)

Model Development. The ultimate objective of the TD system is to perform a simple conversion from TD temperature curves to vapor pressure for the aerosols of interest. However, there are currently many unknowns concerning the actual properties of ambient particles and how they may behave inside a TD system. To address these unknowns and to provide a useful product from the TD system, we have developed a microphysical model that describes the particle evolution inside the TD system. We utilized the one-dimensional modeling approach similar to our previous modeling work [*Wong, et al.*, 2008]. The velocity-averaged temperature and velocity profiles obtained from CFD in Task 1 are used as inputs to the model.

In this microphysical model, the time (t) evolution of a particle radius (r_p) is described using classical evaporation equations [*Seinfeld and Pandis*, 1998] in the free molecule regime ($r_p << \lambda$, where λ is the molecular mean free path in the air):

$$\frac{d(r_p)}{dt} = \frac{M(P_a - P_\infty)}{\rho\sqrt{2\pi MkT}} \qquad (1a)$$

and in the continuum regime ($r_p >> \lambda$):

$$\frac{d(r_p)}{dt} = \frac{D_v M(P_a - P_\infty)}{\rho r_p kT} \qquad (1b)$$

where M and ρ are the molecular weight and condensed-phase density of the evaporating compound, D_v, P_a, and P_∞ are the gas-phase diffusivity, partial pressure and equilibrium vapor pressure for a particle with radius r_p, k is the Boltzmann's constant, and T is the flow temperature in a TD. The model assumes evaporation coefficients are equal to 1 for all compounds, an assumption that fits the data for single component particles.

The time evolution of the gas-phase mass fraction of the evaporating compound (Y) can be described as:

$$\frac{dY}{dt} = \left.\frac{dY}{dt}\right|_{evaporation} + \left.\frac{dY}{dt}\right|_{adsorption} \quad (2)$$

where the two terms on the right hand side of the equation correspond to contributions from particle evaporation and adsorption to activated charcoal, respectively. The particle evaporation term is derived from the classical evaporation equations, and the rate of adsorption to the activated charcoal in the charcoal section is estimated using a simple diffusion equation.

We also include particle loss due to eddy diffusion of particles from high concentration regions (i.e., flow centerline) to low concentration regions (i.e., tube walls), particle loss due to inertial impaction on the walls, and thermophoretic loss due to transport of particles from high temperature regions to low temperature regions.

Model Results. In Phase I of this project, we have applied the above 1-D microphysical modeling approach to simulate particle evolution in a TD system to support our TD development for aerosol volatility measurements. Three of the hydrocarbon species, decandioic (sebacic) acid, hexanedioic (adipic) acid, and dioctyl sebacate (DOS), examined in the laboratory in Task 3 were chosen as model compounds. Our simulation results were compared against experimental data, and parametric effects of flow rates, initial particle size and initial particle concentration were investigated.

Figure 11 shows a comparison of modeled and experimental TD ratio, which is

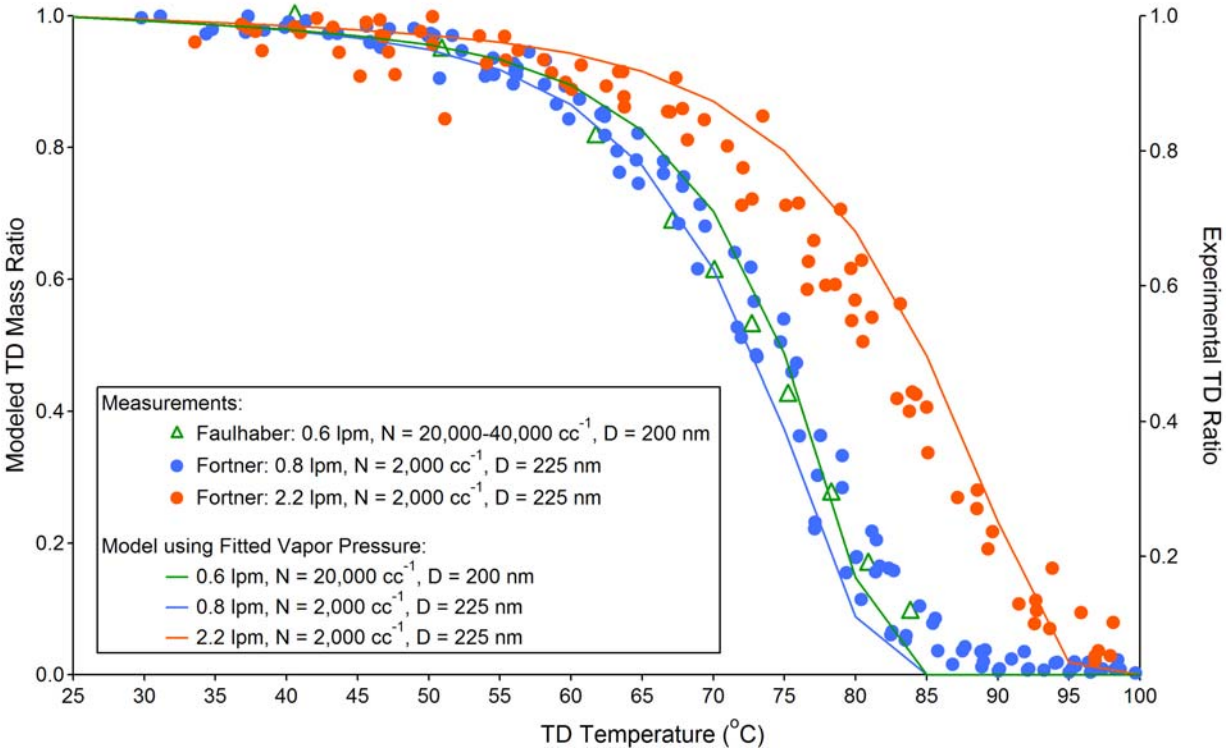

Figure 11. Comparison of the modeled sebacic acid TD curves against experimental data.

the fraction of the particle mass remaining after heating in the TD, as a function of TD temperature (i.e., the highest temperature inside the TD) for sebacic acid. Three different flow rates, 0.6 lpm, 0.8 lpm, and 2.2 lpm were studied and different particle size and number concentration were chosen as initial conditions for each case to match experimental settings. The vapor pressure was used as a fitting parameter in the model for the blue data points. The vapor pressure determined from the fit to the blue points was then used in the model for the green and red data points. As shown in the figure, our 1-D microphysical model is able to capture the experimental observations reasonably well. Our model is also able to predict the effects of flow rates in a TD system (blue versus red curves and symbols), where lower flow rates result in longer residence time inside the TD, allowing particles to have more time to evaporate into smaller size under a given wall temperature. Similar results were obtained comparing model and experimental measurements for adipic acid (a much higher vapor pressure) and di-octyl sebacate (DOS, an intermediate vapor pressure).

Since saturation vapor pressure increases dramatically with increasing temperature, the drop off temperature and the shape of a TD curve are very sensitive to the vapor pressure values used in the simulations. Figure 12 shows literature vapor pressure values as a function of temperature summarized by Chattopadhyay and Ziemann [2005]. Vapor pressures were obtained using three different experimental approaches, temperature programmed thermal desorption (TPTD), tandem differential mobility analyzer (TDMA, Rader and McMurry [1986]) and effusion techniques [*Davies and Malpass*, 1961], as well as a group contribution computational method (SPARC). The vapor pressure from our fit of the microphysical model to our TD experimental data with a flow rate of 0.8 lpm (blue symbols in Figure 11) is also plotted with a dashed line in the left panel of the figure. It is obvious that large uncertainties exist for available sebacic acid vapor pressure values. However, vapor pressures predicted from our model fitting are within a reasonable range. A similar comparison for adipic acid is shown in the right panel of Figure12. These results show that our model not only has the capability to predict experimental TD curves given a known vapor pressure, but also can be used to

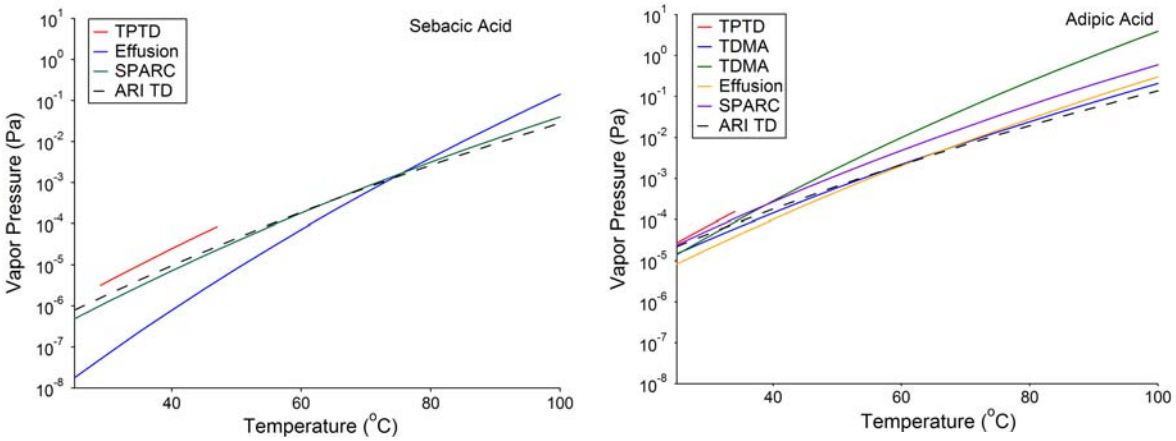

Figure 12. Left panel. Sebacic acid vapor pressures reported in the literature and determined from fitting the microphysical model to the experimental TD data. Right panel. Adipic acid vapor pressures from the literature and from the model fit to the data.

"back calculate" the vapor pressure from the TD data of any arbitrary semi-volatile species.

We conducted a set of parametric studies on initial particle size (*D*) and number concentration (*N*). Two different initial mass loading were studied, and each mass loading was initiated using different initial particle size and number concentration. The model results showed that particles with the same mass loading evaporate faster if they are smaller, evidenced by faster drops in the TD curves. These model results are in good agreement with the experimental data presented in Figure 10 for ammonium sulfate.

The data shown in Figure 11 were obtained with similar particles sizes for the different flow and concentration conditions. We also modeled data for which the particle size was significantly different and found good agreement between the model and the measurements. These results, along with the results discussed above, offer further confirmation that our model is capable of capturing particle evaporation microphysics in a TD system. This also suggests that the developed model serves as an excellent tool for guiding experimental planning. Furthermore, our model is capable of providing advanced understanding of design variables so that the development of an improved thermodenuder system for aerosol volatility measurements can be facilitated.

Bibliography & References Cited

An, W. J., R. K. Pathak, B.-H. Lee, and S. N. Pandis (2007), Aerosol volatility measurement using an improved thermodenuder: Application to secondary organic aerosol, *Journal of Aerosol Science*, *38* 305 – 314.

Andreae, M. O., and A. Gelencser (2006), Black carbon or brown carbon? The nature of light-absorbing carbonaceous aerosols, *Atmos. Chem. Phys*, *6*, 3131-3148.

Baltensperger, U., M. Kalberer, J. Dommen, D. Paulsen, M. R. Alfarra, H. Coe, R. Fisseha, A. Gascho, M. Gysel, S. Nyeki, M. Sax, M. Steinbacher, A. S. H. Prevot, S. Sjoegren, E. Weingartner, and R. Zenobi (2005), Secondary organic aerosols from anthropogenic and biogenic precursors, *Faraday Discuss.*, *130*,, 265–278.

Bilde, M., and S. N. Pandis (2001), Evaporation rates and vapor pressures of individual aerosol species formed in the atmospheric oxidation of alpha- and beta-pinene, *Environmental Science & Technology*, *35*, 3344-3349.

Biswas, S., L. Ntziachristos, K. F. Moore, and C. Sioutas (2007), Particle volatility in the vicinity of a freeway with heavy-duty diesel traffic, *Atmospheric Environment*, *41*, 3479-3493.

Bond, T. C., G. Habib, and R. W. Bergstrom (2006), Limitations in the enhancement of visible light absorption due to mixing state, *J. Geophys. Res*, *111*, D20211.

Bond, T. C., D. G. Streets, K. F. Yarber, S. M. Nelson, J. H. Woo, and Z. Klimont (2004), A technology-based global inventory of black and organic carbon emissions from combustion, *J. Geophys. Res*, *109*, D14203.

Burtscher, H., U. Baltensperger, N. Bukowiecki, P. Cohn, C. Huglin, M. Mohr, U. Matter, S. Nyeki, V. Schmatloch, N. Streit, and E. Weingartner (2001), Separation of volatile and non-volatile aerosol fractions by thermodesorption: instrumental development and applications, *Journal of Aerosol Science*, *32*, 427-442.

Cappa, C. D., E. R. Lovejoy, and A. R. Ravishankara (2007), Determination of evaporation rates and vapor pressures of very low volatility compounds: A study of the C4-C10 and C12 dicarboxylic acids, *Journal of Physical Chemistry A*, *111*, 3099-3109.

Chapman, S., T. G. Cowling, and D. Burnett (1990), *The mathematical theory of non-uniform gases*, Cambridge University Press, Cambridge, UK.

Chattopadhyay, S., H. J. Tobias, and P. J. Ziemann (2001), A method for measuring vapor pressures of low-volatility organic aerosol compounds using a thermal desorption particle beam mass spectrometer, *Analytical Chemistry*, *73*, 3797-3803.

Chattopadhyay, S., and P. J. Ziemann (2005), Vapor pressures of unsubstituted and substituted monocarboxylic and dicarboxylic acids measured using an improved thermal desorption particle beam mass spectrometry method, *Aerosol Sci. Technol.*, *39* 1085-1100.

Chin, M., R. A. Kahn, and S. E. Schwartz (2009), CCSP 2009: Atmospheric Aerosol Properties and Climate Impacts, A Report by the U.S. Climate Change Science Program and the Subcommittee on Global Change Research, 128 pp, National Aeronautics and Space Administration, Washington, D. C.

Clarke, A. D., N. C. Ahlquist, and D. S. Covert (1987), The Pacific marine aerosol: evidence for natural acid sulfates, *J Geophys Res-Atmos*, *92*, 4179-4190.

Davies, M., and V. E. Malpass (1961), Heats of Sublimation of Straight-Chain Monocarboxylic Acids, *J. Chem. Soc.*, 1048-1055.

de Gouw, J. A., A. M. Middlebrook, C. Warneke, P. D. Goldan, W. C. Kuster, J. M. Roberts, F. C. Fehsenfeld, D. R. Worsnop, M. R. Canagaratna, A. A. P. Pszenny, W. C. Keene, M. Marchewka, S. B. Bertman, and T. S. Bates (2005), The Budget of Organic Carbon in a Polluted Atmosphere: Results from the New England Air Quality Study in 2002, *J. Geophys Res.*, *110*, doi:10.1029/2004JD005623.

Denkenberger, K. A., R. C. Moffet, J. C. Holecek, T. P. Rebotier, and K. A. Prather (2007), Real-time, single-particle measurements of oligomers in aged ambient aerosol particles, *Environmental Science & Technology*, *41*, 5439-5446.

Donahue, N. M., A. L. Robinson, C. O. Stanier, and S. N. Pandis (2006), Coupled partitioning, dilution, and chemical aging of semivolatile organics, *Environmental Science & Technology*, *40*, 2635-2643.

Fierz, M., M. G. C. Vernooij, and H. Burtscher (2007), An improved low-flow thermodenuder, *Journal of Aerosol Science*, *38*, 1163-1168.

Fuzzi, S., M. O. Andreae, B. J. Huebert, M. Kulmala, T. C. Bond, M. Boy, S. J. Doherty, A. Guenther, M. Kanakidou, and K. Kawamura (2006), Critical assessment of the current state of scientific knowledge, terminology, and research needs concerning the role of organic aerosols in the atmosphere, climate, and global change, *Atmos. Chem. Phys*, *6*, 859-860.

Hamilton, J. F., P. J. Webb, A. C. Lewis, J. R. Hopkins, S. Smith, and P. Davy (2004), Partially oxidised organic components in urban aerosol using GCXGC-TOF/MS, *Atmos. Chem. Phys.*, *4*, 1279-1290.

Heald, C. L., D. J. Jacob, R. J. Park, L. M. Russell, B. J. Huebert, J. H. Seinfeld, H. Liao, and R. J. Weber (2005), A large organic aerosol source in the free troposphere missing from current models, *Geophysical Research Letters*, *32*, 4.

Huffman, J. A., A. C. Aiken, K. S. Docherty, I. M. Ulbrich, P. F. DeCarlo, J. T. Jayne, T. B. Onasch, A. Trimborn, D. R. Worsnop, P. J. Ziemann, and J. L. Jimenez (2007), Volatility of primary and secondary organic aerosols in the field contradicts current model representations, *Geophys. Res. Lett.*, *submitted*.

Huffman, J. A., K. S. Docherty, A. C. Aiken, M. J. Cubison, I. M. Ulbrich, P. F. DeCarlo, D. Sueper, J. T. Jayne, D. R. Worsnop, and P. J. Ziemann (2009a), Chemically-resolved aerosol volatility measurements from two megacity field studies, *Atmos. Chem. Phys. Discuss*, *9*, 2645-2697.

Huffman, J. A., P. J. Ziemann, J. T. Jayne, D. R. Worsnop, and J. L. Jimenez (2008), Development and Characterization of a Fast-Stepping/Scanning Thermodenuder for Chemically-Resolved Aerosol Volatility Measurements, *Aerosol Science and Technology*, *42*, 395–407.

Huffman, J. A., P. J. Ziemann, J. T. Jayne, D. R. Worsnop, and J. L. Jimenez (2009b), Correction to "Development and Characterization of a Fast-Stepping/Scanning Thermodenuder for Chemically-Resolved Aerosol Volatility Measurements", *Aerosol Science and Technology*, *43*, 273.

Jacobson, M. C., K. J. Hansson, and R. J. Charlson (2000), Organic atmospheric aerosols: review and state of the science, *Rev. of Geophys.*, *38*, 267-294.

Jacobson, M. Z. (2004), Climate response of fossil fuel and biofuel soot, accounting for soot's feedback to snow and sea ice albedo and emissivity, *J. Geophys. Res*, *109*.

Jayne, J. T., D. C. Leard, X. Zhang, P. Davidovits, K. A. Smith, C. E. Kolb, and D. R. Worsnop (2000), Development of an Aerosol Mass Spectrometer for Size and Composition Analysis of Submicron Particles, *Aerosol Sci. Technol.*, *33*, 49-70.

Johnson, D., S. R. Utembe, M. E. Jenkin, R. G. Derwent, G. D. Hayman, M. R. Alfarra, H. Coe, and G. McFiggans (2006), Simulating regional scale secondary organic aerosol formation during the TORCH 2003 campaign in the southern UK, *Atmospheric Chemistry and Physics*, *6*, 403-418.

Jonsson, A. M., M. Hallquist, and H. Saathoff (2007), Volatility of secondary organic aerosols from the ozone initiated oxidation of alpha-pinene and limonene, *Journal of Aerosol Science*, *38*, 843-852.

Kalberer, M., D. Paulsen, M. Sax, M. Steinbacher, J. Dommen, A. S. H. Prevot, R. Fisseha, E. Weingartne, V. Frankevich, R. Zenobi, and U. Baltensperger (2004), Identification of polymers as major components of atmospheric organic aerosols, *Science*, *303*, 1659-1662.

Kanakidou, M., J. H. Seinfeld, S. N. Pandis, I. Barnes, F. J. Dentener, M. C. Facchini, R. Van Dingenen, B. Ervens, A. Nenes, C. J. Nielsen, E. Swietlicki, J. P. Putaud, Y. Balkanski, S. Fuzzi, J. Horth, G. K. Moortgat, R. Winterhalter, C. E. L. Myhre, K. Tsigaridis, E. Vignati, E. G. Stephanou, and J. Wilson (2005), Organic aerosol and global climate modelling: a review, *Atmospheric Chemistry and Physics*, *5*, 1053-1123.

Lelieveld, J., P. J. Crutzen, V.Ramanathan, M.O.Andreae, C. A. M. Brenninkmeijer, T. Campos, G. R. Cass, R. R. Dickerson, H. Fischer, J. A. de Gouw, A. Hansel, A. Jefferson, D. Kley, A. de Laat, S. Lal, M. G. Lawrence, J. M. Lobert, O. L. Mayol-Bracero, A. P. Mitra, T. Novakov, S. J. Oltmans, K. A. Prather, T. Reiner, H. Rodhe, H. A. Scheeren, D. Sikka, and J. Williams (2001), The Indian Ocean Experiment: Widespread Air Pollution from South and Southeast Asia, *Science*, *291*, 1031-1036.

Madl, P. (2003), Instrumental development and application of a thermodenuder, 193 pp, Salzburg University, Salzburg, Austria and Queensland University of Technicology, Brisbane, Australia.

Menon, S., J. Hansen, L. Nazarenko, and Y. Luo (2002), Climate Effects of Black Cargon Aerosols in China and India, *Science*, *297*, 2250-2253.

Meyer, N. K., J. Duplissy, M. Gysel, A. Metzger, J. Dommen, E. Weingartner, M. R. Alfarra, A. S. H. Prevot, C. Fletcher, and N. Good (2009), Analysis of the hygroscopic and volatile properties of ammonium sulphate seeded and unseeded SOA particles, *Atmos. Chem. Phys*, *9*, 721-732.

Prakash, M. J., M. Prasad, and K. Srinivasan (2000), Modeling of thermal conductivity of charcoal–nitrogen adsorption beds, *Carbon*, *38*, 907–913.

Rader, D. J., and P. H. McMurry (1986), Application of the Tandem Differential Mobility Analyzer to Studies of Droplet Growth or Evaporation, *Journal of Aerosol Science*, *17*, 771-787.

Ramanathan, V., and G. Carmichael (2008), Global and regional climate changes due to black carbon, *Nature Geoscience*, *1*, 221-227.

Ramanathan, V., P. J. Cruzen, J. T. Kiehl, and D. Rosenfeld (2001), Aerosols, Climate, and the Hydrological Cycle, *Science*, *294*, 2119-2124.

Ramanathan, V., F. Li, M. V. Ramana, P. S. Praveen, D. Kim, C. E. Corrigan, H. Nguyen, E. A. Stone, J. J. Schauer, G. R. Carmichael, B. Adhikary, and S. C. Yoon (2007a), Atmospheric brown clouds: Hemispherical and regional variations in long-range transport, absorption, and radiative forcing, *J. Geophys. Res.*, *112*, D22S21 (26).

Ramanathan, V., M. V. Ramana, G. Roberts, D. Kim, C. Corrigan, C. Chung, and D. Winker (2007b), Warming trends in Asia amplified by brown cloud solar absorption, *Nature*, *448*, 575-578.

Robinson, A. L., N. M. Donahue, M. K. Shrivastava, E. A. Weitkamp, A. M. Sage, A. P. Grieshop, T. E. Lane, J. R. Pierce, and S. N. Pandis (2007), Rethinking Organic Aerosols: Semivolatile Emissions and Photochemical Aging, *Science*, *315*, 1259-1262.

Schnaiter, M., C. Linke, O. Mohler, K. H. Naumann, H. Saathoff, R. Wagner, U. Schurath, and B. Wehner (2005), Absorption amplification of black carbon internally mixed with secondary organic aerosol, *J. Geophys. Res*, *110*.

Schwarz, J. P., J. R. Spackman, D. W. Fahey, R. S. Gao, U. Lohmann, P. Stier, L. A. Watts, D. S. Thomson, D. A. Lack, and L. Pfister (2008), Coatings and their enhancement of black carbon light absorption in the tropical atmosphere, *J. Geophys. Res*, *113*.

Seinfeld, J. H., and S. N. Pandis (1998), *Atmospheric Chemistry and Physics: From Air Pollution to Climate Change*, John Wiley and Sons, Inc., New York.

Shrivastava, M. K., E. M. Lipsky, C. O. Stanier, and A. L. Robinson (2006), Modeling semivolatile organic aerosol mass emissions from combustion systems, *Environmental Science & Technology*, *40*, 2671-2677.

Solomon, S., D. Qin, M. Manning, R. B. Alley, T. Berntsen, N. L. Bindoff, Z. Chen, A. Chidthaisong, J. M. Gregory, G. C. Hegerl, M. Heimann, B. Hewitson, B. J. Hoskins, F. Joos, J. Jouzel, V. Kattsov, U. Lohmann, T. Matsuno, M. Molina, N. Nicholls, J. Overpeck, G. Raga, V. Ramaswamy, J. Ren, M. Rusticucci, R. Somerville, T. F. Stocker, P. Whetton, R. A. Wood, and D. Wratt (2007), Climate Change 2007: The Physical Science Basis. Contribution of Working Group I to the Fourth Assessment Report of the Intergovernmental Panel on Climate Change, Cambridge University Press, Cambridge, United Kingdom and New York, NY, USA.

Stone, E. A., G. C. Lough, J. J. Schauer, P. S. Praveen, C. E. Corrigan, and V. Ramanathan (2007), Understanding the origin of black carbon in the atmospheric brown cloud over the Indian Ocean, *J. Geophys Res.*, *112*, D22S23.

Tobias, H. J., and P. J. Ziemann (1999), Compound Identification in Organic Aerosols Using Temperature-Programmed Thermal Desorption Particle Beam Mass Spectrometry, *Analytical Chemistry*, *71*, 3428-3435.

Volkamer, R., J. L. Jiménez, F. San Martini, K. Dzepina, Q. Zhang, D. Salcedo, L. T. Molina, D. R. Worsnop, and M. J. Molina (2006), Secondary Organic Aerosol Formation from Anthropogenic Air Pollution: Rapid and Higher than Expected, *Geophys. Res. Lett.*, *33*, L17811, doi:17810.11029/12006GL026899.

Wehner, B., S. Philippin, and A. Wiedensohler (2002a), Design and calibration of a thermodenuder with an improved heating unit to measure the size-dependent volatile fraction of aerosol particles, *Journal of Aerosol Science*, *33* 1087–1093.

Wehner, B., S. Philippin, and A. Wiedensohler (2002b), Design and calibration of a thermodenuder with an improved heating unit to measure the size-dependent volatile fraction of aerosol particles, *J. Aerosol Science*, *33*, 1087-1093.

Wehner, B., S. Philippin, A. Wiedensohler, V. Scheer, and R. Vogt (2004), Variability of non-volatile fractions of atmospheric aerosol particles with traffic influence, *Atmospheric Environment*, *38*, 6081-6090.

Wong, H. W., P. E. Yelvington, M. T. Timko, T. B. Onasch, R. C. Miake-Lye, J. Zhang, and I. A. Waitz (2008), Microphysical Modeling of Ground-Level Aircraft-Emitted Aerosol Formation: Roles of Sulfur-Containing Species, *Journal of Propulsion and Power*, *24*, 590.

Wu, Z., L. Poulain, B. Wehner, A. Wiedensohler, and H. Herrmann (2009), Characterization of the volatile fraction of laboratory-generated aerosol particles by thermodenuder-Aerosol Mass Spectrometer coupling experiments, *Journal of Aerosol Science*, *article in press*.

Zhang, Q., J. L. Jiménez, M. R. Canagaratna, J. D. Allan, H. Coe, I. Ulbrich, M. R. Alfarra, A. Takami, A. M. Middlebrook, Y. L. Sun, K. Dzepina, E. Dunlea, K. Docherty, P. F. DeCarlo, D. Salcedo, T. Onasch, J. T. Jayne, T. Miyoshi, A. Shimono, S. Hatakeyama, N. Takegawa, Y. Kondo, J. Schneider, F. Drewnick, S. Borrmann, S. Weimer, K. Demerjian, P. Williams, K. Bower, R. Bahreini, L. Cottrell, R. J. Griffin, J. Rautiainen, J. Y. Sun, Y. M. Zhang, and D. R. Worsnop (2007), Ubiquity and dominance of oxygenated species in organic aerosols in anthropogenically—influenced Northern Hemisphere midlatitudes, *Geophys. Res. Lett.*, *34*, L13801, doi:13810.11029/12007GL029979.